

XMM-Newton confirmation of a new intermediate polar: XMMU J185330.7-012815

C. Y. Hui^{1*}, K. Sriram² and C.-S. Choi²

¹*Department of Astronomy and Space Science, Chungnam National University, Daejeon 305-764, Republic of Korea*

²*International Center for Astrophysics, Korea Astronomy and Space Science Institute, 36-1 Hwam, Yuseong, Daejeon 305-348, Republic of Korea*

Received 2011 March 14

ABSTRACT

We report the results from a detailed spectro-imaging and temporal analysis of an archival XMM-Newton observation of a new intermediate polar XMMU J185330.7-012815. Its X-ray spectrum can be well-described by a multi-temperature thermal plasma model with the K-lines of heavy elements clearly detected. Possible counterparts of XMMU J185330.7-012815 have been identified in optical and UV bands. The low value of the inferred X-ray-to-UV and X-ray-to-optical flux ratios help to safely rule out the possibility as an isolated neutron star. We confirm the X-ray periodicity of ~ 238 s but, different from the previous preliminary result, we do not find any convincing evidence of phase-shift in this observation. We further investigate its properties through an energy-resolved temporal analysis and find the pulsed fraction monotonically increases with energy.

Key words: binaries: close — cataclysmic variables — stars: individual (XMMU J185330.7-012815, G31.9-1.1) — X-rays: stars

1 INTRODUCTION

XMMU J185330.7-012815 is an X-ray object that has its emission nature not yet completely confirmed. It has been detected in the ROSAT All-Sky Survey (RASS). Based on its extent inferred from the RASS data (i.e. 11 arcmin \times 7 arcmin), Schaudel (2003) has suggested that XMMU J185330.7-012815, which was designated as G31.9-1.1 in their work, to be a candidate of supernova remnant (SNR) in our Galaxy. Schaudel (2003) have further analysed the X-ray properties of XMMU J185330.7-012815 by using an archival ASCA observation in which XMMU J185330.7-012815 located at an off-axis angle of ~ 14 arcmin. Although they found that XMMU J185330.7-012815 appears to be elongated in an ASCA GIS image, the large off-axis angle precludes any constraining spatial analysis. Examining the spectral data collected by ASCA, Schaudel (2003) found that the X-ray spectrum of XMMU J185330.7-012815 is featureless and can be fitted with an absorbed power-law model with a photon index of $\Gamma = 1.84^{+0.23}_{-0.21}$ (cf. Table 5.2 in Schaudel 2003). Together with the apparently centrally-brightened X-ray morphology, the author claimed that the power-law spectral fit strongly supports the interpretation of a center-filled SNR or a Crab-like SNR. However, with only ~ 1100 source counts from the ASCA

data, one cannot unambiguously distinguish between the power-law model and a single-temperature thermal plasma model with $kT = 5.23^{+1.88}_{-1.35}$ keV (Schaudel 2003). Also, the non-detection of any radio emission from the position of XMMU J185330.7-012815 makes the SNR interpretation questionable.

In an archival search for the Galactic magnetars, Munro et al. (2008) have made use of 506 archival Chandra data and 441 archival XMM-Newton data. This search has included a dedicated XMM-Newton observation of XMMU J185330.7-012815 with an off-axis angle of only ~ 0.4 arcmin. Interestingly, the authors have detected a signal with a period of ~ 238 s from this observation. With this discovery, instead of being a magnetar candidate, Munro et al. (2008) have suggested this source is probably an accreting white dwarf. The cataclysmic variable nature of this source is further supported by the optical spectroscopy performed by J. Halpern & E. Gotthelf (private communication reported in Munro et al. 2008).

Although Munro et al. (2008) have identified XMMU J185330.7-012815 as a promising candidate of cataclysmic variable, they have not further analysed and discussed the nature of this object as this is out of the scope of their work. To confirm the X-ray emission properties of XMMU J185330.7-012815, a detailed spectro-imaging and temporal analysis of the aforementioned XMM-Newton observation is required and this provides the motivation of

* E-mail: cyhui@cnu.ac.kr

this investigation. In §2, we are going to describe the details of this XMM-Newton observation of XMMU J185330.7-012815 as well as the procedure of the data reduction. The method and the results of the data analysis are presented in §3. Finally, we will discuss the implication and the possible nature of XMMU J185330.7-012815 as an accreting white dwarf.

2 OBSERVATION & DATA REDUCTION

XMMU J185330.7-012815 was observed by XMM-Newton on 25-26 October 2004 (Observation ID: 0201500301). The X-ray data used in this investigation were obtained with the European Photon Imaging Camera (EPIC) on board XMM-Newton (Jansen et al. 2001). EPIC consists of two Metal Oxide Semiconductor (MOS1/2) CCD detectors (Turner et al. 2001) of which half of the beam from two of the three X-ray telescopes is reflected to. The other two halves of the incoming photon beams are reflected to a grating spectrometer (RGS) (den Herder et al. 2001). The third of the three X-ray telescopes is dedicated to expose the EPIC-PN CCD detector solely (Strüder et al. 2001). The EPIC-PN CCD was operated in small-window mode with a medium filter to block optical stray light. This data provide imaging spectral and temporal information. All recorded events are time-tagged with a temporal resolution of 5.7 ms. The MOS1/2 CCDs were setup to operate in full-window mode with a medium filter in each camera. The MOS1/2 cameras provide imaging, spectral and timing information, though the later with a temporal resolution of 2.6 s only.

The aimpoint of the satellite in this observation is RA=18^h53^m29.7^s and Dec=-01°28'31.8" (J2000). With the most updated instrumental calibration, we generate the event lists from the raw data obtained from all EPIC instruments with the tasks *emproc* and *epproc* of the XMM Science Analysis Software (XMMSAS version 9.0.0). Examining the raw data from the EPIC-PN CCD, we did not find any timing anomaly which was observed in many of the XMM-Newton data sets (cf. Hui & Becker 2006 and references therein). This provides us with opportunities for an accurate timing analysis. We then created filtered event files for the energy range 0.2 keV to 12 keV for all EPIC instruments and selected only those events for which the pattern was between 0–12 for MOS cameras and 0–4 for the EPIC-PN camera. We further cleaned the data by accepting only the good times when sky background was low and removed all events potentially contaminated by bad pixels. After the filtering, the effective exposures are found to be 19.5 ks and 13.5 ks for MOS1/2 and EPIC-PN respectively.

Apart from the X-ray data, we have also made use of the Optical Monitor (OM, Mason et al. 2001) data obtained in standard imaging mode with two filters UVW1 (an effective wavelength of 2910 Å) and UVM2 (2310 Å). The OM data are reduced by using the standard XMMSAS *omichain* task. For imaging and source detection, the track history was created, bad pixels were removed and the resulting image was subsequently used for source detection. Since individual photons were centroid to one eighth of detector pixel by onboard electronics which produces a noise pattern known as *modulus 8* spatial fixed pattern noise and hence this noise was overcome using *ommodmap* task. The

source detection was performed by using the task *omdetect* and counts were converted into magnitudes for the corresponding filters with the aid of the task *ommag*. The UV bandpass counts were converted into fluxes using the recipe provided by Alice Breeveld.¹

3 DATA ANALYSIS

3.1 Spatial Analysis

The composite MOS1/2 image of a 6' × 6' field around XMMU J185330.7-012815 is shown in Figure 1. XMMU J185330.7-012815 is observed as the brightest object in this field. We determined its position and significance by means of a wavelet detection algorithm. The X-ray position is found to be RA=18^h53^m30.708(5)^s, Dec=-01°28'16.00(6)" [J2000], where the numbers in the parentheses indicate the 1 σ statistical uncertainties of the last digit. The signal-to-noise ratio of XMMU J185330.7-012815 is found to be 326 σ ². This MOS1/2 image clearly rules out the claim of extended source as suggested by the RASS data (Schaudel 2003). There are two serendipitous X-ray sources found in the vicinity of XMMU J185330.7-012815, where are labeled as sources A and B in Figure 1. The wavelet detection reports the locations and the significances of these sources to be (RA=18^h53^m34.68(2)^s, Dec=-01°27'38.6(4)" [J2000]; $S/N = 6\sigma$) and (RA=18^h53^m32.24(2)^s, Dec=-01°26'29.9(3)" [J2000]; $S/N = 17\sigma$) for sources A and B respectively. Since our focus is on characterising the emission nature of XMMU J185330.7-012815, we will not discuss the properties of these two sources further in this paper.

3.2 Spectral Analysis

We estimated the effects of pileup in all EPIC data by using the XMMSAS task *epatplot*. Our results showed that all the EPIC data were not affected by CCD pileup. In order to maximize the signal-to-noise ratio for XMMU J185330.7-012815, we extracted its source spectrum from circles with a radius of 50" and 30" in the MOS1/2 and EPIC-PN cameras respectively. This choice of extraction regions corresponds to the encircled energy fraction of $\sim 90\%$ in all cameras³ and at the same time it minimizes the contamination from the nearby X-ray sources. The background spectra were sampled from the nearby regions with circles of a radius of 60" and 40" in MOS1/2 and EPIC-PN respectively. Response files were computed for all datasets by using the XMMSAS tasks *rmfgen* and *arfgen*. After the background subtraction, we have 9130±97 cts, 9314±98 cts, and 19282±140 cts collected for the spectral analysis from MOS1, MOS2 and EPIC-PN cameras respectively.

In order to constrain the spectral parameters tightly, we

¹ http://xmm.esac.esa.int/sas/7.0.0/watchout/Evergreen_tips_and_tricks/uvflux.sh

² The source significances quoted in this paper are in units of Gehrels error: $\sigma_G = 1 + \sqrt{C_B} + 0.75$ where C_B is the background counts.

³ http://xmm.esac.esa.int/external/xmm_user_support/documentation/uhb/node17.html

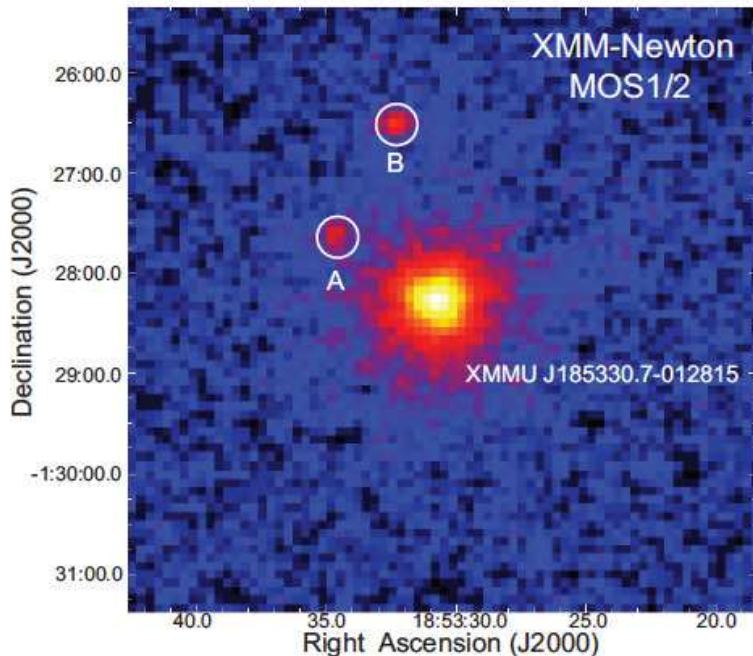


Figure 1. The raw X-ray image of the $6' \times 6'$ field-of-view centered at XMMU J185330.7-012815 generated by merging the MOS1 and MOS2 data in the energy range of 0.2 – 12 keV. Two serendipitous unidentified sources are also detected in this FOV.

fitted the data obtained from three cameras simultaneously. For the spectrum extracted from each camera, we grouped the data so as to have at least 50 counts per bin. We found there are fluctuations in the spectral data below 0.3 keV that can be ascribed to the undesirable spectral response. Therefore, we limited all the spectral analysis in the energy range 0.3 – 12 keV. All the spectral fits are performed with XSPEC 12.5.1. The parameters of the best-fit models are summarized in Table 1. All quoted errors are 1σ for 2 parameters of interest.

The X-ray spectrum of XMMU J185330.7-012815 as observed by XMM-Newton is displayed in Figure 2 which has shown the line features suggesting K-lines of heavy elements, in particular the features at ~ 6.7 keV and ~ 6.9 keV. This has led us to examine the spectrum with emission model of hot plasma that includes line emissions from different elements. First, we attempted to fit the spectrum with MEKAL which is a code that models the plasma in collisional ionization equilibrium (Mewe et al. 1985). With the metal abundances fixed at the solar values, a single temperature MEKAL model results in a hydrogen equivalent column density of $n_H = (4.6 \pm 0.3) \times 10^{20} \text{ cm}^{-2}$ and a plasma temperature of $kT = 6.4 \pm 0.2$ keV with a goodness-of-fit of $\chi^2_\nu = 1.89$ (583 D.O.F.). The large χ^2_ν indicates that this model is unlikely to be the adequate description of the data. In examining the fitting residuals, we have identified the systematic deviations at energies larger than ~ 5 keV and smaller than ~ 1 keV. This prompts us to examine the spectrum with multi-temperature plasma model.

With a two-temperature MEKAL model, the best-fit yields a similar absorption of $n_H = 4.7^{+0.3}_{-0.4} \times 10^{20} \text{ cm}^{-2}$ and the plasma temperatures of $kT_1 = 1.00^{+0.04}_{-0.03}$ keV and $kT_2 =$

$8.34^{+0.40}_{-0.42}$ keV. In comparison with the single-temperature model, the goodness-of-fit, $\chi^2_\nu = 1.27$ (581 D.O.F.), is found to be improved significantly. Statistically, the additional component is required at a confidence level $> 99.9\%$. Although the systematic residuals at energies > 5 keV and < 1 keV are not observed in this two-temperature model, we notice that this model appears to overpredict the emission at the energies around ~ 1 keV and ~ 6.7 keV. This leads us to speculate that either the abundances of the metals that give rise to the line emissions at these energies are different from their solar values or the data require an additional component for modeling. For testing the first hypothesis, we further analysed the X-ray spectrum of XMMU J185330.7-012815 by taking metal abundance as free parameter in the fitting. As the residuals at these energies are likely to be due to Fe K α and L lines, we take the abundance of iron as a fitting parameter.

By entangling the free parameters of Fe abundances in both components, we found the residuals at ~ 1 keV and ~ 6.5 keV can be minimized. The goodness-of-fit is improved ($\chi^2_\nu = 1.20$, 580 D.O.F.). The model yields the column density of $n_H = (5.7 \pm 0.4) \times 10^{20} \text{ cm}^{-2}$, the plasma temperatures of $kT_1 = 0.81 \pm 0.03$ keV and $kT_2 = 7.75^{+0.44}_{-0.65}$ keV, as well as an iron abundance of $\text{Fe} = 0.72 \pm 0.08$. Although the residuals of the lines can be reduced with this model, with a more careful examination, we found that there are still discrepancies between the observed data and this model at energies larger than ~ 7 keV. This leads us to consider the other possibility, namely whether there is any additional spectral component is required to model this data.

Comparison between the best-fit three-temperature plasma model and the observed data is shown in Figure 2. There is no systematic deviation between the data and this model within the entire adopted energy range. The goodness-of-fit is further improved ($\chi^2_\nu = 1.07$, 579 D.O.F.). Different from the two-temperature model, we do not find any significant deviation of the Fe abundance from the solar value in this adopted model. Therefore, we fixed all the metal abundances at the solar values in three-temperature plasma model. It results in the column density of $n_H = (5.5 \pm 0.4) \times 10^{20} \text{ cm}^{-2}$, the plasma temperatures of $kT_1 = 0.65 \pm 0.04$ keV, $kT_2 = 1.78^{+0.39}_{-0.15}$ keV and $kT_3 = 10.84^{+1.40}_{-0.96}$ keV. The unabsorbed flux inferred by this model is $f_X = (6.4 \pm 0.5) \times 10^{-12} \text{ ergs cm}^{-2} \text{ s}^{-1}$ in 0.3 – 12 keV.

We notice that there is a class of cataclysmic variable which contains a soft blackbody component (cf. Evans & Hellier 2007). Statistically the soft blackbody component is only required at a confidence level of $\sim 10\%$ in this observed spectrum. Therefore, we do not consider this spectral contribution in this work.

The ASCA and XMM-Newton spectra of XMMU J185330.7-012815 appear to be qualitatively different. ASCA observations show no line emission features and the spectrum with a single power-law model and obtained a reasonable goodness-of-fit with the ASCA data ($\chi^2_\nu = 0.86$, 40 D.O.F.) (Schaudel 2003). However, with the photon statistic improved by a factor of ~ 34 , the spectral data obtained by XMM-Newton clearly show the presence of the emission line features. Fitting a power-law to the EPIC spectrum does not result in an acceptable goodness-of-fit ($\chi^2_\nu = 1.72$, 583 D.O.F.). Similar to the

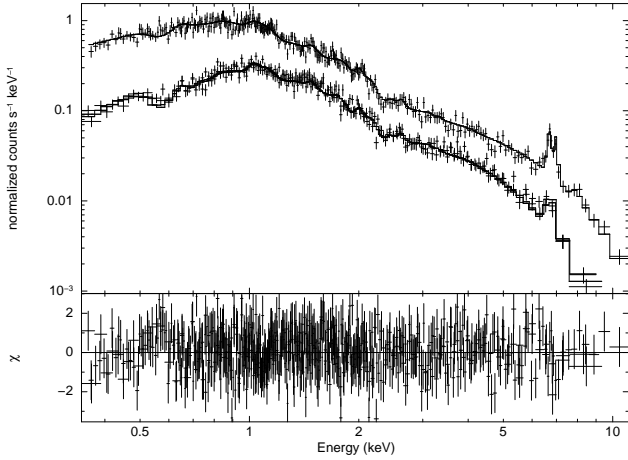


Figure 2. Energy spectrum of XMMU J185330.7-012815 as observed with the EPIC-PN (upper spectrum) and MOS1/2 detectors (lower spectra) and simultaneously fitted to an absorbed three-temperatures MEKAL model (upper panel) and contribution to the χ^2 fit statistic (lower panel).

single-temperature plasma model, it cannot describe the data below ~ 2 keV and above ~ 5 keV. Such discrepancy between the inferences drawn from these two observations can be ascribed to the relatively poor quality of ASCA data.

3.3 Temporal Analysis

3.3.1 Modulation Period

To confirm the X-ray period by Munro et al. (2008), we did a periodicity search by using an epoch folding method after converting the X-ray arrival times to the barycentric times of the solar system. The best period, which was determined by fitting a Gaussian function to the centroid of χ^2 -peak, is $P = 238.1 \pm 0.1$ s for both PN and MOS data under the assumption that the pulses are coherent (where the errors in χ^2 are included and the MOS1 and MOS2 data are combined). This period is consistent with the result reported by Munro et al. (2008). If we take the possible irregularity of the pulses into account, then the error should increase to $P = 238.1 \pm 1.1$ s in which the error is the standard deviation σ of the Gaussian function fitted to the full χ^2 -profile.

Munro et al. (2008) have also pointed out that the phases vary by ≈ 0.1 cycles with a timescale of ≈ 5000 s which suggests the incoherent nature of the source. We have also carried out the phase analysis by dividing the PN light curve into 4 segments with a timescale of ≈ 5000 s and folded each segment at the period of 238.1 s over the epoch MJD 53303.98674 (Figure 3). By fitting a sinusoidal model to the data (see below), we obtained the following peak positions in time order: $1.13^{+0.02}_{-0.03}$, $1.05^{+0.06}_{-0.07}$, $1.06^{+0.03}_{-0.04}$, and $1.14^{+0.07}_{-0.09}$ in phases (where the errors are at the 90% confidence level). Taking the uncertainties into account, we are not able to unambiguously state whether there is a clear, systematic phase shift. Furthermore, by running a χ^2 -test among each pair of the time-sliced light curves in Figure 3, their distributions are found to be consistent with each other at a confidence level $> 99.9\%$. Therefore, we conclude that no convincing

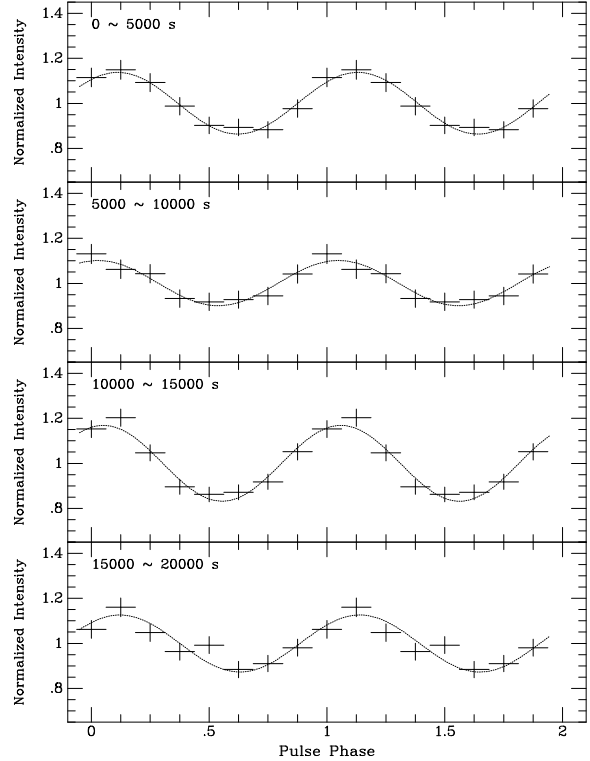


Figure 3. Pulse (or modulation) profiles for time-sliced PN data. The data (*plus signs*) were folded at the period 238.1 s from the epoch MJD 53303.98674. The pulse phase has been repeated over two cycles. A sine curve plus a constant (*dotted curve*) was fitted to the profiles.

evidence for the incoherence can be found in our independent analysis.

3.3.2 Energy-Resolved Folded Light Curves

A pulse or modulation profile folded at the period of 238.1 s shows a single broad peak over one cycle of the data. It can be approximated by a sinusoidal model plus a constant unpulsed level:

$$A \sin(2\pi[\phi - \phi_0]) + C. \quad (1)$$

To see how the profiles vary with energy, we investigate the energy-resolved profiles obtained in three different energy bands, 0.2–1.2 keV, 1.2–3.0 keV, and 3.0–10 keV. For this analysis, we focus on the PN dataset as it provides the superior photon statistic in each of the considered energy bands. Figure 4 shows the profiles (plus signs), where the backgrounds are not subtracted (the extracted backgrounds from a photon deficit region in the same CCD chip are very small and they are at most $\sim 2\%$ level compared to their source count rates). We fit the sinusoidal model to the profiles with allowing all the parameters to be free and obtain the following results from the best-fit parameters. Goodness of the model-fit is given in each panel of the Figure 4. These profiles show no significant phase shift in the chosen energy bands. The pulse amplitude $2A$ (cf. Equation 1) is found to increase with increasing energy: 0.16 ± 0.03 (0.2 - 1.2 keV), 0.34 ± 0.04 (1.2 - 3.0 keV), and 0.46 ± 0.06 (3.0 - 10 keV). In the other words, a pulsed (or modulation) fraction (i.e.

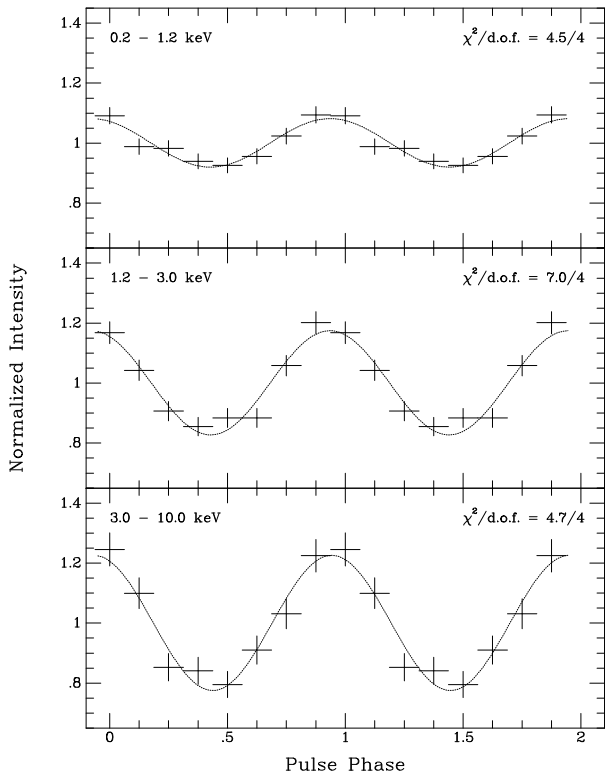


Figure 4. Energy-resolved pulse profiles of XMMU J185330.7-012815 for PN data. The data were folded at the period 238.1 s from the observation start time. The intensity in each panel was normalized by the average count rates of the same energy band. The pulse phase has been repeated over two cycles. A sine curve plus a constant (*dotted curve*) was fitted to the profiles (*plus signs*).

A/C) increases from $8\% \pm 2\%$ to $23\% \pm 3\%$ with increasing energy. All the quoted errors for the temporal results are at the 90% confidence level.

3.4 Analysis of Optical Monitor (OM) data

Within $10''$ from the X-ray position of XMMU J185330.7-012815, we have detected two UV sources in the OM data. One UV source (hereafter U1) has found to have the magnitudes of $m_{UVW1}=15.99\pm 0.02$ and $m_{UVM2}=16.49\pm 0.03$ with the corresponding significances of 68.31σ and 53.46σ respectively. On the other hand, the other source (hereafter U2) has the magnitudes of $m_{UVW1}=15.98\pm 0.03$ and $m_{UVM2}=18.86\pm 0.26$ with the corresponding significances of 43.81σ and 6.70σ respectively. The corrected count rate of U1 and U2 for both filters are $c_1=3.06\pm 0.06$ cts/s (UVW1), $c_1=0.82\pm 0.03$ cts/s (UVM2) and $c_2=1.92\pm 0.05$ cts/s (UVW1), $c_2=0.06\pm 0.01$ cts/s (UVM2) respectively. We subsequently use these count rates to calculate the UV fluxes. For the conversion factors in the UVW1 and UVM2 bandpass of 4.76×10^{-16} erg cm $^{-2}$ cts $^{-1}$ Å $^{-1}$ and 2.20×10^{-15} erg cm $^{-2}$ cts $^{-1}$ Å $^{-1}$, we obtain the fluxes of $(4.36\pm 0.06)\times 10^{-12}$ erg cm $^{-2}$ s $^{-1}$ and $(4.16\pm 0.03)\times 10^{-12}$ erg cm $^{-2}$ s $^{-1}$ for U1 in the corresponding filters. For U2, the fluxes are found to be $(2.66\pm 0.05)\times 10^{-12}$ erg cm $^{-2}$ s $^{-1}$ and $(0.30\pm 0.01)\times 10^{-12}$ erg cm $^{-2}$ s $^{-1}$ in UVW1 and UVM2 respectively.

Of these two detected UV sources, U1 is found to have its position coincided with the nominal X-ray position of XMMU J185330.7-012815. Furthermore, while there is no optical counterpart can be found for U2, we have identified an optical source in *B*-band at the position of U1 (see §4). The X-ray-to-UV flux ratio is found to have the same order-of-magnitude as the X-ray-to-optical flux ratio. In view of these properties, we suggest U1 is more likely to be the counterpart of XMMU J185330.7-012815.

4 DISCUSSION & SUMMARY

In this paper, we present a detailed spectro-imaging and temporal analysis of an archival XMM-Newton observation of XMMU J185330.7-012815, which has its emission nature not yet been identified unambiguously.

We found that the energy spectrum of XMMU J185330.7-012815 obtained by the EPIC can be well-described by an absorbed multi-temperature plasma model. The inferred column density is $n_H \sim 5 \times 10^{20}$ cm $^{-2}$ which is far lower than the total Galactic neutral hydrogen absorption, $n_H \sim 10^{22}$ cm $^{-2}$, in the direction towards XMMU J185330.7-012815 (Kalberla et al. 2005; Dickey & Lockman 1990). This leads us to rule out the extragalactic origin of XMMU J185330.7-012815.

The unabsorbed X-ray flux inferred from the best-fit model is found to be $f_X \sim 6 \times 10^{-12}$ ergs cm $^{-2}$ s $^{-1}$. Together with the UV counterpart identified in OM, the inferred X-ray-to-UV flux ratio is $f_X/f_{UV} \sim 1.5$. To further constrain the source nature, we also search for any optical identification of XMMU J185330.7-012815 in the United States Naval Observatory (USNO)-B1.0 catalogue (Monet et al. 2003). Within the 20σ X-ray positional uncertainty of XMMU J185330.7-012815 (see §3.1), we have identified one optical counterpart with $B = 17.11$. The position of this source is also found to be consistent with that of U1. By using the n_H inferred from the X-ray analysis to estimate the foreground extinction, we calculate the extinction-corrected optical flux in *B*-band as $f_B = 1.8 \times 10^{-12}$ ergs cm $^{-2}$ s $^{-1}$ which implies $f_X/f_B \sim 3.8$. Such low value of X-ray-to-optical flux ratio can safely rule out the possibility as an isolated neutron star which typically has $f_X/f_B > 10^3$ (cf. Haberl 2007).

Through our independent search for the periodic X-ray signal from XMMU J185330.7-012815, we have identified a peak at ~ 238.1 s in the power density spectrum. This has confirmed the periodicity firstly reported by Munro et al. (2008). Nevertheless, different from the result reported by Munro et al. (2008), we do not find any convincing phase shift in our phase analysis. In any case, it is unlikely that this signal with such long period comes from rotation-powered pulsars (cf. Manchester et al. 2005). Instead, we speculate this periodic signal is possibly from a white dwarf. By comparing the uncovered period with the typical values of accreting white dwarf binaries, we further suggest that it is likely to be the spin period of the white dwarf and does not correspond to an orbital period⁴. This interpretation is further supported by the spectral properties. The X-ray

⁴ <http://asd.gsfc.nasa.gov/Koji.Mukai/iphome/catalog/alpha.html>

spectrum of XMMU J185330.7-012815 can be described by a three-temperature plasma model and clearly shows the presence of iron lines, which have often been seen in one type of accreting white dwarf binaries, namely the intermediate polars (IPs) (e.g. Patterson 1994; Cropper et al. 2002). The additional frequencies in the X-ray power spectra which corresponds to orbital or the beat period is absent in XMMU J185330.7-012815. In the context of an IP interpretation, this suggests that material accretes onto the pole via a disk.

Although the spin period and the spectral properties strongly favor the IP interpretation, the observed property of monotonically increasing modulation with increasing energy in the light curves requires a further discussion. In contrast to XMMU J185330.7-012815, many IPs show an opposite trend of decreasing modulation with energy (e.g. Norton & Watson 1989) which is generally explained by the variation of photoelectric absorption in the accretion curtain across the observer's line of sight (Rosen, Mason, & Córdoba 1988). The accretion rate is expected to have the maximum from the sector of the disc that is closest to the magnetic pole and fall off with deviation from this sector. This gives rise to a continuous variation of column density along the cross-section of the curtain and hence results in the modulation by photoelectric absorption. The minimum of the light curve is thus at the phase when the accreting pole, where the absorption is the largest, is pointing toward the observer. As the effect of photoelectric absorption is more prominent in the soft band than in the hard band, a trend of decreasing pulsed fraction with increasing photon energy is not unexpected in this scenario (cf. Figure 9 in Rosen et al. 1988).

Although the behaviour of decreasing amplitude with increasing energy has been observed in many IPs, a number of them do deviate from this general trend. For example, a clear increase in amplitude modulation with increasing energy is also found in V2306 Cygni (WGA J1958.2+3232) by the ASCA observation (Norton et al. 2002). Norton & Mukai (2007) found that an IP candidate XY Ari also shows an increasing modulation with increasing energy in the XMM-Newton data, whereas it shows a decreasing behaviour with increasing energy in the RXTE data (see Figure 1 and Figure 5 in Norton & Mukai 2007). Another IP that shows a modulation different from the general trend is IGR J00234+6141 in the RXTE observations (see Table 2 in Butters et al. 2011). However, the XMM-Newton/EPIC-PN observation of this object shows no modulation above 2 keV (Anzolin et al. 2009). There is another IP, PQ Gem, which shows an increasing modulation in sub-divided low energy bands and a decreasing modulation in high energy bands of ASCA and RXTE observations (James et al. 2002). On the other hand, a few other IPs show a constant modulation in RXTE observations (e.g. Butters et al. 2007, 2008) and some show no amplitude modulation in the EPIC-PN energy band (e.g. de Martino et al. 2005). Since a diversity of temporal behaviour has been observed, energy dependency of amplitude modulation is a weaker criterion to constrain the property of an IP.

To further probe the temporal behaviour of XMMU J185330.7-012815, we have also analysed the archival RXTE observations for this source (ObsIDs: 90070-04-01-00, 90070-04-01-01, 90070-04-01-02, 90070-04-02-00,

90070-04-02-01 and 90070-04-02-02). However, no pulsed signal from XMMU J185330.7-012815 was detected from all these datasets. On the other hand, we found that the emission line features at ~ 6.5 keV in the RXTE PCA spectrum. Hence, we speculate that the non-detection of pulsation in the RXTE data can be ascribed to the lack of imaging capability in resolving the source in a crowded region. The upcoming missions with focusing optics for hard X-rays, such as NuSTAR (Harrison et al. 2010), will certainly provide the appropriate instruments for further investigation of this interesting IP candidate.

The X-ray spectra of many IPs are described by a complex absorption model as expected in the context of accretion curtain (e.g. Ramsay et al. 2008). However, such additional absorption component is not required in modeling the spectrum of XMMU J185330.7-012815. The lack of complex and high absorption in XMMU J185330.7-012815 might indicate a low inclination angle such that the observed X-rays are not passing through the accretion curtains. On the other hand, the observed hydrogen column density (i.e. $n_{\text{H}} \sim 5 \times 10^{20} \text{ cm}^{-2}$) is much lower than typically observed in other IPs (cf. Ezuka & Ishida 1999). The absence of high values of absorption can possibly due to the low accretion rate. Such low absorption have also been seen in several cases, such as HT Cam (de Martino et al. 2005), EX HYa (Mukai et al. 2003) and V1025 Cen (Hellier et al. 1998) along with a few other IP sources in which a strong soft component was always prominent (Evan & Hellier 2007). Nevertheless, such soft component is not observed in the case of XMMU J185330.7-012815. In the scenario of a low inclination angle, the missing soft component may simply due to the geometrical effect (Evan & Hellier 2007). Alternatively, this component might be much softer than the spectral coverage of XMM-Newton EPIC so that it is not revealed in this observation.

The spectral results of XMMU J185330.7-012815 suggest a relatively low shock temperature of ~ 11 keV (cf. Table 1). Very recently, Yuasa et al. (2010) have investigated the shock temperatures of 15 IPs and found two sources also with low temperatures, FO Aqr (~ 14 keV) and EX Hya (~ 12 keV). In another systematic study of 23 IPs, the lowest temperature is found to be ~ 12 keV for the source DO Dra (Brunscheiger et al. 2009). Furthermore, we notice that the temperature of a new IP RX J0704 has exhibited a change from a high value of > 44 keV to ~ 11 keV in eight months (Anzolin et al. 2008). There is an IP, AE Aqr, which shows exceptionally low temperatures plasma of 0.1 - 7 keV (e.g. Choi et al. 1999; Choi & Dotani 2006; Mauche 2009). However, for AE Aqr, it is widely believed that most of the transferred material from the companion does not reach the magnetic poles due to a magnetic propeller effect (e.g., Wynn et al. 1997; Choi & Dotani 2006). Based on aforementioned temperature distribution in IPs, it is clear that the observed temperature of XMMU J185330.7-012815 is not significantly different from a few other IPs and also the observed low plasma temperature may not be persistent. A frequent monitoring of this source is encouraged.

In summary, based on our temporal and spectral analysis, we suggest that XMMU J185330.7-012815 belongs to the IP sub-classification of cataclysmic variables. We would like to stress that, including XY Ari, there are only 8 IPs/IP candidates which show spin period less than 240 s. Owing to

this small population, the exact selection criteria to classify a source as an IP is not well-defined for this short-period sub-class, which so far can only be constrained on the basis of the six observational criteria given by Patterson (1994). It is not certain if all six of these characteristics should be exhibited by an IP. For a further investigation of this new IP, a multi-wavelength observation campaign is required to unveil the physical and geometrical configuration of this system. In particular, the determination of the orbital period of this source through a dedicated optical observation will definitely play a key role in determining the system parameters such as orbital inclination. Furthermore, a dedicated series of X-ray observations is desirable to search for the possible eclipses from XMMU J185330.7-012815. Through the timing of the eclipse ingress and egress, one is able to determine the size of the X-ray emitting region and hence put an additional observational constraint on the emission nature of this system.

ACKNOWLEDGMENTS

The authors would like to thank the anonymous referee for the useful comments. CYH is supported by the research fund of Chungnam National University in 2011.

REFERENCES

- Anzolin G., de Martino D., Bonnet-Bidaud J. M., Mouchet M., Gansicke B. T., Matt G., Mukai K., 2008, *A&A* 489, 1243
- Anzolin G., de Martino D., Falanga M., Mukai K., Bonnet-Bidaud J.-M., Mouchet M., Terada Y., Ishida M., 2009, *A&A*, 501, 1047
- Brunschweiler J., Greiner J., Ajello M., Osborne M., 2009, *A&A* 496, 121
- Butters O. W., Barlow E. J., Norton A. J., Mukai K., 2007, *A&A*, 475, L29
- Butters O. W., Norton A. J., Hakala P., Mukai K., Barlow E. J., 2008, *A&A*, 487, 271
- Butters O. W., Norton A. J., Mukai K., Tomsick J. A., 2011, *A&A* 526 77
- Choi C. S., Dotani T., Agrawal P. C., 1999, *ApJ*, 525, 399
- Choi C. S., Dotani T., 2006, *ApJ*, 646, 1149
- Cropper M., Ramsay G., Hellier C., Mukai K., Mauche C., Pandel D., 2002, *Proc. R. Soc. London A*, 360, 1951
- den Herder et al., 2001, *A&A*, 365, 7
- de Martino D., Matt G., Mukai K., Bonnet-Bidaud J.-M., Gansicke B. T., Gonzalez Perez J. M., Haberl F., Mouchet M., Solheim J.-E., 2005, *A&A*, 437, 935
- Dickey J. M., Lockman F. J., 1990, *ARAA*, 28, 215
- Evans P. A., Hellier C., 2007, *ApJ*, 663, 1277
- Ezuka H., Ishida M., 1999, *ApJS*, 120, 277
- Haberl F., 2007, *Ap&SS*, 308, 181
- Harrison F. A., et al., 2010, *SPIE*, 7732, 27
- Hellier C., Beardmore A. P., Buckley, D. A. H., 1998, *MNRAS*, 29, 851
- Hui C. Y., Becker W., 2006, *A&A*, 454, 543
- James Cynthia H., Ramsay G., Cropper M., Branduardi-Raymont G., 2002, *MNRAS*, 336, 550
- Jansen F., et al., 2001, *A&A*, 365, L1
- Kalberla P. M. W. et al., 2005, *A&A*, 440, 775
- Manchester R. N., Hobbs G. B., Teoh A., Hobbs M., 2005, *AJ*, 129, 1993
- Mason K. O., et al., 2001, *A&A*, 365, L36
- Mauche C. W., 2009, *ApJ*, 706, 130
- Mewe R., Gronenschild E. H. B. M., van den Oord G. H. J., 1985, *A&AS*, 62, 197
- Monet D., et al., 2003, *AJ*, 125, 984
- Mukai K., Kinkhabwala A., Peterson J. R., Kahn S. M., Paerels F., 2003, *ApJ*, 586, L77
- Muno M. P., Gaensler B. M., Nechita A., Miller J. M., Slane, P. O., 2008, *ApJ*, 680, 639
- Norton A. J., Watson M. G., 1989, *MNRAS*, 237, 853
- Norton A. J., Quaintrell H., Katajainen S., Lehto H. J., Mukai K., Negueruela I., 2002, *A&A*, 384, 195
- Norton A. J., Mukai K., 2007, *A&A*, 472, 225
- Patterson J., 1994, *PASP*, 106, 209
- Ramsay G., Wheatley P. J., Norton A. J., Hakala P., Baskill D., 2008, *MNRAS*, 387, 1157
- Rosen S. R., Mason K. O., Córdova F. A., 1988, *MNRAS*, 231, 549
- Schaudel D., 2003, PhD thesis, Ludwig-Maximilians Universität München
- Strüder L., et al., 2001, *A&A*, 365, L18
- Turner M. J. L., et al., 2001, *A&A*, 365, L27
- Wynn G. A., King A. R., Horne, K., 1997, *MNRAS*, 286, 436
- Yuasa T., Nakazawa K., Makishima K., Saitou K., Ishida M., Ebisawa K., Mori H., Yamada S., 2010, *A&A*, 520, 25

Table 1. Best-fit spectral parameters of XMMU J185330.7-012815.

	MEKAL	MEKAL+MEKAL	MEKAL+MEKAL	MEKAL+MEKAL+MEKAL	PL
n_H (10^{20} cm $^{-2}$)	4.60 ± 0.31	$4.74^{+0.34}_{-0.35}$	$5.67^{+0.42}_{-0.40}$	$5.46^{+0.40}_{-0.38}$	$12.08^{+0.57}_{-0.56}$
kT_1 (keV)	6.42 ± 0.23	$1.00^{+0.04}_{-0.3}$	0.81 ± 0.03	0.65 ± 0.04	-
kT_2 (keV)	-	$8.34^{+0.40}_{-0.42}$	$7.75^{+0.44}_{-0.65}$	$1.78^{+0.39}_{-0.15}$	-
kT_3 (keV)	-	-	-	$10.84^{+1.40}_{-0.96}$	-
Fe ^a	-	1.0 (fixed)	0.72 ± 0.08	1.0 (fixed)	-
Γ	-	-	-	-	1.84 ± 0.02
Norm ₁ ^b	$(2.92 \pm 0.03) \times 10^{-3}$	$(1.46^{+0.18}_{-0.16}) \times 10^{-4}$	$(1.55^{+0.22}_{-0.20}) \times 10^{-4}$	$(8.56^{+1.23}_{-0.87}) \times 10^{-5}$	-
Norm ₂ ^b	-	$(2.70^{+0.03}_{-0.04}) \times 10^{-3}$	$(2.78 \pm 0.04) \times 10^{-3}$	$(3.56^{+1.56}_{-0.75}) \times 10^{-4}$	-
Norm ₃ ^b	-	-	-	$(2.46^{+0.14}_{-0.07}) \times 10^{-3}$	-
Norm _{PL} ^c	-	-	-	-	$(1.07 \pm 0.02) \times 10^{-3}$
χ^2	1099.53	737.50	698.87	621.20	1003.51
D.O.F.	583	581	580	579	583

^aThe abundance of iron relative to the solar photospheric values.

^bThe normalization of MEKAL model is expressed as $(10^{-14}/4\pi D^2) \int N_e N_H dV$ where D is the source distance in cm and N_e and N_H are the electron and hydrogen densities in cm $^{-3}$.

^cThe normalization of the power-law model (PL) at 1 keV in units of photons keV $^{-1}$ cm $^{-2}$ s $^{-1}$.

This paper has been typeset from a \TeX / \LaTeX file prepared by the author.